International Journal of Nanomedicine Dovepress

Open Access Full Text Article ORIGINAL RESEARCH

Elucidating the Mechanism of Large-Diameter Titanium Dioxide Nanotubes in Protecting Osteoblasts Under Oxidative Stress Environment: The Role of Fibronectin and Albumin Adsorption

Yun Xiang[1,2,*], Dini Lin[1,*], Qiang Zhou[1], Hongyu Luo[1], Zixin Zhou[1], Shuyi Wu[2], Keyuan Xu[2], Xiaoting Tang[1], Pingping Ma[2], Chunyuan Cai[1], Xinkun Shen[1]

[1]Wenzhou Key Laboratory for the Diagnosis and Prevention of Diabetic Complications, The Third Affiliated Hospital of Wenzhou Medical University (Ruian People's Hospital), Wenzhou, 325016, People's Republic of China; [2]School and Hospital of Stomatology, Wenzhou Medical University, Wenzhou, 325027, People's Republic of China

*These authors contributed equally to this work and share first authorship

Correspondence: Xinkun Shen; Chunyuan Cai, Wenzhou Key Laboratory for the Diagnosis and Prevention of Diabetic Complications, The Third Affiliated Hospital of Wenzhou Medical University (Ruian People's Hospital), Wenzhou, Zhejiang Province, 325016, People's Republic of China, 108# Wansong Road, Email shenxinkun123@wmu.edu.cn; caichunyuan123@wmu.edu.cn

Background: Large-diameter titanium dioxide nanotubes (TNTs) have shown promise in preserving osteoblast function under oxidative stress (OS) in vitro. However, their ability to enhance osteogenesis in vivo under OS conditions and the underlying mechanisms remain unclear.

Purpose: This study aimed to evaluate the osteogenic potential of 110 nm TNTs (TNT110) compared to 30 nm TNTs (TNT30) in an aging rat model exhibiting OS, and to investigate the mechanisms involved.

Methods: Surface properties of TNTs were characterized, and in vitro and in vivo experiments were conducted to assess their osteoinductive effects under OS. Transcriptomic, proteomic analyses, and Western blotting were performed to investigate the protective mechanisms of TNT110 on osteoblasts. Protein adsorption studies focused on the roles of fibronectin (FN) and albumin (BSA) in modulating osteoblast behavior on TNT110.

Results: In both in vitro and in vivo experiments, TNT110 significantly improved new bone formation and supported osteoblast survival under OS conditions. Subsequent ribonucleic acid sequencing results indicated that TNT110 tended to attenuate inflammatory responses and reactive oxygen species (ROS) expression while promoting endoplasmic reticulum (ER) stress and extracellular matrix receptor interactions, all of which are crucial for osteoblast survival and functionality. Further confirmation indicated that the cellular behavior changes of osteoblasts in the TNT110 group could only occur in the presence of serum. Moreover, proteomic analysis under OS conditions revealed the pivotal roles of FN and BSA in augmenting TNT110's resistance to OS. Surface pretreatment of TNT110 with FN/BSA alone could beneficially influence the early adhesion, spreading, ER activity, and ROS expression of osteoblasts, a trend not observed with TNT30.

Conclusion: TNT110 effectively protects osteoblast function in the OS microenvironment by modulating protein adsorption, with FN and BSA synergistically enhancing osteogenesis. These findings suggest TNT110's potential for use in implants for elderly patients.

Keywords: osteoporosis, oxidative stress, titania nanotube, protein adsorption, osteogenesis

Introduction

Titanium (Ti) and its alloys are heralded for biomedical implants due to excellent biocompatibility, mechanical properties, and corrosion resistance.[1] These attributes have made them popular for oral restoration procedures. Currently, Ti-based implants display effective osseointegration and high success rates. However, compared to the middle-aged and

Received: 22 July 2024
Accepted: 17 October 2024
Published: 22 October 2024

young population, the time required for early osseointegration in elderly implant patients is significantly prolonged.[2] Increasing evidence suggests a close link between the production of reactive oxygen species (ROS) and aging.[3] In the context of implantation, successful osseointegration is crucial for maintaining enduring implant functionality and ensuring the overall success of oral implant procedures.[4] Yet, in elderly patients, the bone microenvironment undergoes abnormal changes, notably marked by increased oxidative stress (OS). This rise in OS is primarily due to elevated levels of ROS, which inflict direct damage on osteoblasts, leading to their deterioration, aging, and apoptosis.[5–7] This, in turn, impedes osteoblast differentiation while simultaneously promoting the proliferation of osteoclasts. Such processes disrupt the dynamic equilibrium between bone formation and resorption, mediated by osteoblasts and osteoclasts, resulting in suboptimal early-stage osseointegration following Ti implantation. This complication often leads to implant instability, increasing the likelihood of implant loosening and failure.[7,8] Therefore, developing surface modification methods for Ti implants with antioxidant properties is key to enhancing its osteoinductive capability in elderly patients.

The surface coating or micro/nano topological modification of Ti implants have been extensively validated as effective approaches to enhance their biological activity.[9,10] Titania nanotubes (TNTs), a common nano-topological structural modification on Ti surfaces, possess controllable geometric parameters and surface morphology similar to natural bone, thereby exhibiting significant bio-activity.[11,12] Moreover, the size of these nanotubes plays a vital role in influencing their biological effects. Previous findings have indicated that in a normal microenvironment, TNTs with a smaller diameter (around 30 nm) favored the adhesion and proliferation of bone marrow mesenchymal stem cells (bMSCs). Conversely, larger diameter TNTs (about 100 nm) facilitated cell spreading, thereby enhancing the osteogenic differentiation capabilities of bMSCs and osteoblasts (MC3T3-E1 cells).[12,13] Nonetheless, it remains unclear whether the mere physical properties of the TNT structure retain similar bone-promoting abilities under OS conditions and the molecular mechanisms involved. Wang et al demonstrated that in an OS microenvironment, 80 nm TNTs could equilibrate ROS expression by generating higher total SOD levels, demonstrating enhanced antioxidant capacity.[14,15] This leaded to the induction of osteogenic differentiation of bMSCs and promoted osseointegration in vivo, surpassing sandblasted and acid-etched surfaces. Our previous study has also proved that under OS, the osteoblasts on 30 nm TNTs (TNT30) exhibited significantly inhibited spreading, proliferation, and osteogenic differentiation.[16] However, 110 nm TNTs (TNT110) were able to maintain osteoblast biological activity by modulating cell adhesion, promoting cytoskeletal reorganization, and upregulating the expression of integrin α5β1 (ITGα5β1).[16] Furthermore, TNT110 showed superior potential in alleviating OS and promoting osteogenic differentiation through the activation of signaling pathways such as FAK/Akt/FoxO3a and Wnt.[16] Although these findings confirmed that TNT110 possesses strong antioxidant potential in vitro, several underlying questions remain to be elucidated: 1) Can TNT110 also protect new bone formation under in vivo OS conditions? 2) Why does TNT110 specifically promote ITGα5β1 expression in an OS microenvironment? 3) Which signaling pathways are systematically regulated by TNT110 to confer oxidative resistance and enhance osteogenic differentiation in osteoblasts under OS? Clarifying these issues will aid in the design and selection of topologically structured titanium materials that are optimal for implant restoration in osteoporosis treatment.

It is widely acknowledged that when biomaterials are implanted into the body and encounter the liquid phase of organisms, free protein molecules from surrounding tissues are rapidly and competitively adsorbed onto the surface of the material, forming a complex protein molecular layer within seconds to minutes.[17] Consequently, cells from adjacent tissues do not directly interact with the surface of the biomaterial. Instead, they respond to the protein layer adsorbed on the material surface, which regulates subsequent cellular reactions.[18] The surface physical and chemical properties of biomaterials, such as charge, wettability, roughness, and chemical groups, influence the type, quantity, and conformation of proteins within this adsorbed protein layer, thereby guiding subsequent cellular responses.[19] The rate of protein adsorption onto the material surface is directly linked to its concentration and molecular weight. Proteins with smaller sizes, higher concentrations, and faster diffusion rates in plasma are initially adsorbed onto the material surface. Over time, larger proteins with stronger adhesive properties can replace these smaller proteins, a phenomenon known as the Vroman effect in protein adsorption.[20,21] Extracellular matrix (ECM) proteins adsorbed on the surface of biomaterials, particularly cell adhesion-related proteins like fibronectin (FN) and vitronectin (VN), bind to transmembrane receptors such as integrin receptors on cell membranes. Binding to specific domains of these proteins triggers signaling from the ECM to the cell interior, initiating the first cell response - adhesion. This response is critical for subsequent cellular

processes, including proliferation, migration, and differentiation.[22] Therefore, we hypothesize that TNTs of different diameters may influence osteoblast-related biological behaviors by modulating protein adsorption on their surface under OS conditions.

In our previous study, we preliminarily confirmed that the antioxidant capability of TNT110 surpasses that of pure titanium and small-diameter TNTs (30 and 70 nm).[16] Notably, the difference between TNT110 and TNT30 was particularly significant, and aside from the variation in diameter (representing a single variable), the physicochemical properties (eg, roughness, crystal structure, wettability, etc.) of these two materials were nearly identical.[16] Therefore, in this study, we selected TNT30 and TNT110 to further investigate the antioxidant effects of different TNTs under OS conditions both in vivo and in vitro and explore their underlying mechanisms. Using transcriptome/proteome sequencing and bioinformatics analysis, we specifically focused on two key proteins, fibronectin (FN) and albumin (BSA), and hypothesized that their competitive adsorption on the surface is crucial for achieving excellent antioxidant stress performance of TNT110. Further research was conducted on the effects of these two proteins on early adhesion, viability, diffusion, endoplasmic reticulum stress (ERS), and endogenous reactive oxygen species (ROS) expression in MC3T3-E1 cells under OS. This comprehensive approach aims to provide insights into the modification of protein coatings with antioxidant functions on the surface of TNTs, thereby potentially improving the success rate of implant repair in patients with osteoporosis.

Materials and Methods

Materials

Pure titanium foil (99.99%) was purchased from Baoji Fuxin Nonferrous Metal Products Co., Ltd. (Shanxi, China). BSA (HPLC, ≥ 98%) and FN (Catalog number: F8180; Specification: 0.2 mg/mL) were obtained from Solarbio Biotechnology Co., Ltd. (Beijing, China). Ammonium fluoride (AR, ≥ 98%), glycerol (AR, ≥ 99%), and hydrogen peroxide solution (H_2O_2, 3%) were purchased from Sigma-Aldrich Co. (Shanghai, China). Reactive oxygen detection kit (Catalog number: S0033S), BCA detection kit (Catalog number: P0010), Alkaline phosphatase (ALP) activity detection kit (Catalog number: P0321M), ER-Tracker Red fluorescent probe (Catalog number: C1041M), and ECL chemiluminescence reagent (Catalog number: P0018M) were provided by Biyuntian Biotechnology Co., Ltd. (Shanghai, China). Other chemical reagents (AR) were purchased from Platinum Strontium Titanium Chemical Reagent Co., Ltd. (Guizhou, China).

Preparation and Characterization of Different TNTs

Initially, Ti sheets were meticulously cleaned using acetone, anhydrous ethanol, and deionized water in an ultrasonic water bath, each for 10 min. The cleaned Ti sheet was then positioned as the anode in an anodizing power supply setup, with a platinum sheet serving as the cathode. The electrolysis was conducted in a glycerol/water mixture (1:1 volume ratio) containing 0.27 M ammonium fluoride for 1 h. By adjusting the voltage to 10 V and 30 V during the anodic oxidation process, surfaces of TNTs with diameters of 30 nm and 110 nm were obtained, named TNT30 and TNT110, respectively. The resulting samples were cut into sizes of 1×1 cm² (suitable for 24-well plates) and 10×10 cm² (suitable for petri dishes). They were sterilized by soaking both sides in a 75% alcohol solution for 1 h on a super-clean table, avoiding ultraviolet irradiation, and then dried for subsequent use.

Field Emission Scanning Electron Microscopy (FE-SEM, Hitachi SU8000, Japan) was employed to examine the surface morphology of each sample. Prior to imaging, samples pre-adsorbed with various proteins were sputter-coated with a thin gold layer to enhance conductivity. The images were captured at an accelerating voltage of 5 kV, with a working distance of approximately 9 mm. Atomic Force Microscopy (AFM, Dimension, Bruker, Germany) was used to assess surface roughness. Scanning was performed with a scan size of 2 μm × 2 μm and a scan rate of 1 hz. The static water contact angle (WCA), indicating the surface wettability of each sample, was measured at ambient temperature using a water contact angle measurement device (DSA30, Kruss, Germany). A 5 μL droplet of deionized water was placed on the material surface and allowed to stand for 10s before the contact angle was recorded. The surface chemical composition was analyzed using X-ray Photoelectron Spectroscopy (XPS, Model PHI5400, Perkin Elmer, USA). XPS spectra were recorded using monochromatic Al Kα radiation, with binding energies calibrated to the C1s peak at 284.8 eV. The crystal structure of the surfaces was

determined using X-ray Diffraction (XRD, SmartLab, Rigaku, Tokyo, Japan). Measurements were carried out using Cu Kα radiation over a 2-theta range of 5° to 90°, with a step size of 0.053°.

Study on the Behavior of Osteoblasts on TNTs Under OS Conditions

Cell Viability Detection

MC3T3-E1 cells (Cell Resource Center, Chinese Academy of Sciences, China) were seeded onto the surfaces of TNT30 and TNT110 samples at a density of 2×10^4 cells/cm². The cells were cultured in alpha-minimum essential medium (α-MEM) supplemented with 1% penicillin-streptomycin, 10% fetal bovine serum (FBS) and 300 μM H_2O_2, consistent with the protocols established in our previous study.[16] After 4 d of incubation, the original medium was discarded, and the wells were replenished with α-MEM medium containing 10% 3-(4,5-Dimethylthiazol-2-yl)-2,5-diphenyltetrazolium bromide (MTT). Following an additional 4 h of incubation, DMSO was added to fully dissolve the formazan crystals for 15 min. The optical density (OD) value of each well was then measured at 490 nm using a microplate reader (Synergy H1, Berton, USA).

In vitro Osteogenic Performance Study

MC3T3-E1 cells were seeded onto the surface of each sample at a density of 2×10^4 cells/cm² and incubated in a 37 °C environment using α-MEM medium supplemented with 300 μM H_2O_2. After 7 d of culture, ALP activity in the MC3T3-E1 cells was quantitatively analyzed using both an ALP activity detection kit and a BCA protein assay kit. Furthermore, following 14 d of cell culture, the cells were fixed in 4% paraformaldehyde for 40 min, and stained with alizarin red solution. The formation of mineralized nodules was observed and photographed under a microscope (E24W, Leica, Germany). The mineralized nodules were then dissolved in 10% cetylpyridinium chloride, and the absorbance at 540 nm was measured using a microplate reader (Synergy H1, Berton, USA) for quantitative analysis.

Local Osteogenic Capacity of TNT Implants in Aging SD Rats

Twelve 18-month-old male SD rats, each weighing approximately 700 g, were randomly divided into two groups: TNT30 (n = 6) and TNT110 (n = 6). All animal experiments were conducted in accordance with the ARRIVE guidelines and strictly adhered to the National Institutes of Health guide for the care and use of Laboratory animals (NIH Publication No. 8023, revised 1978). Additionally, the study received approval from the Ethics Committee of Ruian People's Hospital (Approval number: SYSQ-2023-022). Titanium implants with different nanotube modifications were implanted into the bilateral femoral epiphyses of the aging SD rats. One month after implant placement, all aged SD rats were executed, and the femoral specimens were collected and fixed in 4% paraformaldehyde. A small animal computed tomography system (micro-CT, SkyScan1276, Bruker, Germany) was applied to scan and evaluate the formation of new bone around the implants. The new bone volume/total volume ratio (BV/TV) and trabecular spacing of bone (Tb.Th) were quantitatively analyzed using CTVox, CTAn and CTVol software.

In vitro Osteoblast Transcriptomic Detection

MC3T3-E1 cells were seeded onto the surfaces of TNT30 and TNT110 samples (10×10 cm²) at a density of 4×10^4 cells/cm² and cultured in α-MEM medium containing 300 μM H_2O_2. After 4 d of culture, cells from each group were harvested using Trizol solution. The collected samples were then sent to Paisennuo Biotechnology Co., Ltd. (Shanghai, China) for RNA sequencing. All the obtained data were processed and analyzed in R software v4.3.0 (https://www.r-project.org/). Firstly, the principal component analyse (PCA) was performed using the prcomp function in R software and visualized using the R package "ggord" to assess the independence of the samples. Subsequently, the data were analyzed for differences us the R packages "limma" and "edgeR" with the screening criteria of $|\text{Log}_2$ Fold Change (Log_2 FC)| > 0.5 and false discovery rate (FDR) < 0.05. Volcano plots and heatmaps were generated with the R packages "pheatmap" and "ggplot2" to show the differentially expressed genes (DEGs). Enrichment analyses of all genes and DEGs, such as Kyoto Encyclopedia of Genes and Genomes (KEGG), Gene Ontology (GO) and Gene Set Enrichment Analysis (GSEA), were performed and processed by the R package 'clusterprofiler'.[23] Finally, mouse gene annotations for this data were obtained from the R package "org.Mm.eg.db".

Study on the Behavior of Osteoblasts Under OS with/without FBS

Cell Adhesion and Spreading

Under the culture conditions of OS without serum (α-MEM medium supplemented with 1% penicillin-streptomycin and 300 μM H_2O_2) or with serum (α-MEM medium supplemented with 1% penicillin-streptomycin, 300 μM H_2O_2, and 10% FBS), MC3T3-E1 cells were seeded onto the surfaces of TNT30 and TNT110 at a density of 4×10^4 cells/cm². After 30 and 120 min of culture, cells were fixed using 4% paraformaldehyde for 40 min, followed by nuclear staining with 4,6-diamino-2-phenyl indole (DAPI) for 5 min. These cells were then observed and imaged using a Leica fluorescence microscope (DMi8, Leica, Germany). Furthermore, after 24 h of cell culture, cells underwent fixation with 4% paraformaldehyde for 40 min. The cytoskeleton and nuclei were subsequently stained with FITC-labeled phalloidin and DAPI for 60 min and 5 min, respectively, allowing for the observation of cell spreading through fluorescence microscopy (DMi8, Leica, Germany). Finally, the number of adherent cells and their spreading area were quantitatively analyzed and statistically assessed using Image J software.

Endogenous ROS Detection

MC3T3-E1 cells were seeded onto the surfaces of TNT30 and TNT110 samples at a density of 4×10^4 cells/cm² under OS conditions with or without FBS. After 24 h, the medium was discarded, and cells were stained with 2',7'-Dichlorodihydrofluorescein diacetate (DCFH-DA) dye. Following a 30 min incubation at 37 °C, the cells were observed and imaged using a fluorescence microscope (DMi8, Leica, Germany). The fluorescence intensity was subsequently quantified using Image J software.

Endoplasmic Reticulum (ER) Staining

MC3T3-E1 cells were also seeded on TNT30 and TNT110 samples at a density of 4×10^4 cells/cm² under OS conditions with or without FBS. Post 24 h of culture, the cells were incubated with the diluted ER-tracker red fluorescent probe at 37 °C for 30 min. The cells were then observed and imaged under a fluorescence microscope (DMi8, Leica, Germany). Finally, the fluorescence intensity was quantified using Image J software.

Investigating the Onset of Osteoblast Adhesion Under OS Conditions

MC3T3-E1 cells were seeded onto the surfaces of TNT30 and TNT110 samples at a density of 4×10^4 cells/cm². These samples were then cultured in α-MEM medium containing 300 μM H_2O_2 in a 37°C incubator for 1, 3, 5, 7, and 9 min, respectively. After the designated time periods, the cells were fixed with 4% paraformaldehyde for 40 min, followed by DAPI staining to facilitate nuclear visualization. The cells were then observed under a fluorescence microscope (DMi8, Leica, Germany). Finally, Image J software was used to quantify the number of adhered cells.

Investigating Serum Protein Adsorption on TNTs Under OS Conditions

Quantitative Analysis of Protein Adsorbed on TNT Surfaces

Based on previous results regarding cell adhesion, a protein pre-adsorption period of 5 minutes was chosen to investigate variations in the types and quantities of surface proteins on each sample. TNT30 and TNT110 samples were incubated in 10% FBS containing 300 μM H_2O_2 at 37°C for 5 min. Following a gentle wash with PBS, proteins were eluted using 1 wt% sodium dodecyl sulfate (SDS) for 1 h. The protein content adsorbed on the surface of each sample group was then collected and quantified using a BCA protein assay kit.

Proteomic Analysis of the Protein Layer Adsorbed on TNTs Surfaces

TNT30 and TNT110 samples were incubated in 10% FBS containing 300 μM H_2O_2 at 37°C for 5 min. After incubation, proteins adsorbed on the surface of each sample were eluted with 1 wt% SDS and collected. Beijing Bio-Tech Pack Technology Co. Ltd. was commissioned to identify and analyze the proteins using Liquid Chromatography-Mass Spectrometry (LC-MS/MS) protein identification technology. Subsequent proteomics-related data were analyzed based on the aforementioned RNA sequencing analysis process (FDR < 0.25). During data screening, proteins with zero abundance expression levels in the samples were excluded to enhance the reliability of the conclusions.

Western Blotting (WB) Experiment

TNT30 and TNT110 samples were incubated in 10% FBS containing 300 μM H_2O_2 at 37°C for 5 min, proteins adsorbed on each sample's surface were collected using the elution method. Proteins were then separated using 8% SDS-polyacrylamide gel electrophoresis (SDS-PAGE) and transferred to a polyvinylidene fluoride (PVDF) membrane. The membrane was blocked at ambient temperature for 1 h with a rapid blocking solution, followed by incubation with FN/BSA monoclonal primary and corresponding secondary antibody solutions. Protein expression levels were detected using an enhanced chemiluminescence (ECL) system. Finally, the grayscale values of the scanned bands were analyzed using Image J software.

Biological Evaluation of Protein Pre-Adsorbed TNTs Under OS Conditions

Preparation of Protein Solution

Based on proteomic identification results, BSA and FN were selected for further experimentation. To align with the protein concentrations in 10% FBS, BSA and FN protein solutions were prepared at concentrations of 4 mg/mL and 20 μg/mL in phosphate-buffered saline (PBS) solution. Additionally, BSA/FN mixed protein solutions were prepared at the physiological concentration ratio (approximately 200:1), resulting in concentrations of 4 mg/mL for BSA and 20 μg/mL for FN.

Physicochemical Pharacterization of Protein Pre-Adsorbed TNTs

For pre-adsorption treatment, the TNT30 and TNT110 samples were immersed for 5 min in protein solutions of BSA, FN, FN/BSA, and 10% FBS, each containing 300 μM H_2O_2. The treated samples were named accordingly: TNT30 (BSA), TNT30(FN), TNT30(FN/BSA), TNT30(FBS), TNT110(BSA), TNT110(FN) TNT110(FN/BSA), TNT110(FBS). FE-SEM was used to characterize the surface morphology of the protein pre-adsorbed samples. A water contact angle measuring instrument assessed the surface wettability post-protein pre-adsorption. XPS was employed to detect changes in surface chemical composition after protein pre-adsorption.

Osteoblast Responses on Protein Pre-Adsorbed TNTs Under OS Conditions

MC3T3-E1 cells were seeded at a density of 4×10^4 cells/cm² onto each protein pre-adsorbed sample under OS and serum-free conditions (α-MEM medium supplemented with 1% penicillin-streptomycin and 300 μM H_2O_2). First, the cell viability was assessed as per section 2.3.1 after incubation periods of 6 and 24 h. Second, the cell adhesion and spreading was evaluated in accordance with section 2.4.1 after 30/120 min and 24 h, respectively. Finally, the ROS and ER levels were assessed following the protocols outlined in sections 2.4.1 and 2.4.3, respectively, after a 24 h period.

Statistic Analysis

All data are presented as mean ± standard deviation (SD). Statistical analysis and graphing of relevant experimental data were carried out using SPSS 25 software and GraphPad Prism 7.0 software. Significant differences were determined using *t*-tests and one-way analysis of variance (ANOVA), with a 95% confidence interval (*$P < 0.05$). Furthermore, the Benjamini-Hochberg method was employed for adjusting multiple comparisons in *P*-adjust values during the multiomics analysis.

Results

Preparation and Characterization of TNTs

Figure 1A depicted the surface structure and roughness of TNTs. The results revealed that both TNT30 and TNT110 samples displayed regular nanotube structures on their surfaces, with average diameters of approximately 30 nm and 110 nm, respectively. They also exhibited similar surface roughness, with Ra approximately 17.2 ± 4.1 nm for TNT30 and 16.3 ± 1.3 nm for TNT110 (Figure 1B). Figure 1C demonstrates that TNT30 and TNT110 samples possessed hydrophilic surfaces, with static WCA values of 14.22 ± 6.36° and 15.59 ± 4.85°, respectively. XRD analysis (Figure 1D) revealed that the titania crystal structures of both TNT30 and TNT110 were amorphous. Furthermore, XPS results (Figure 1E) showed that the surfaces of both TNT30 and TNT110 comprised Ti, O, and C elements, with no significant difference in

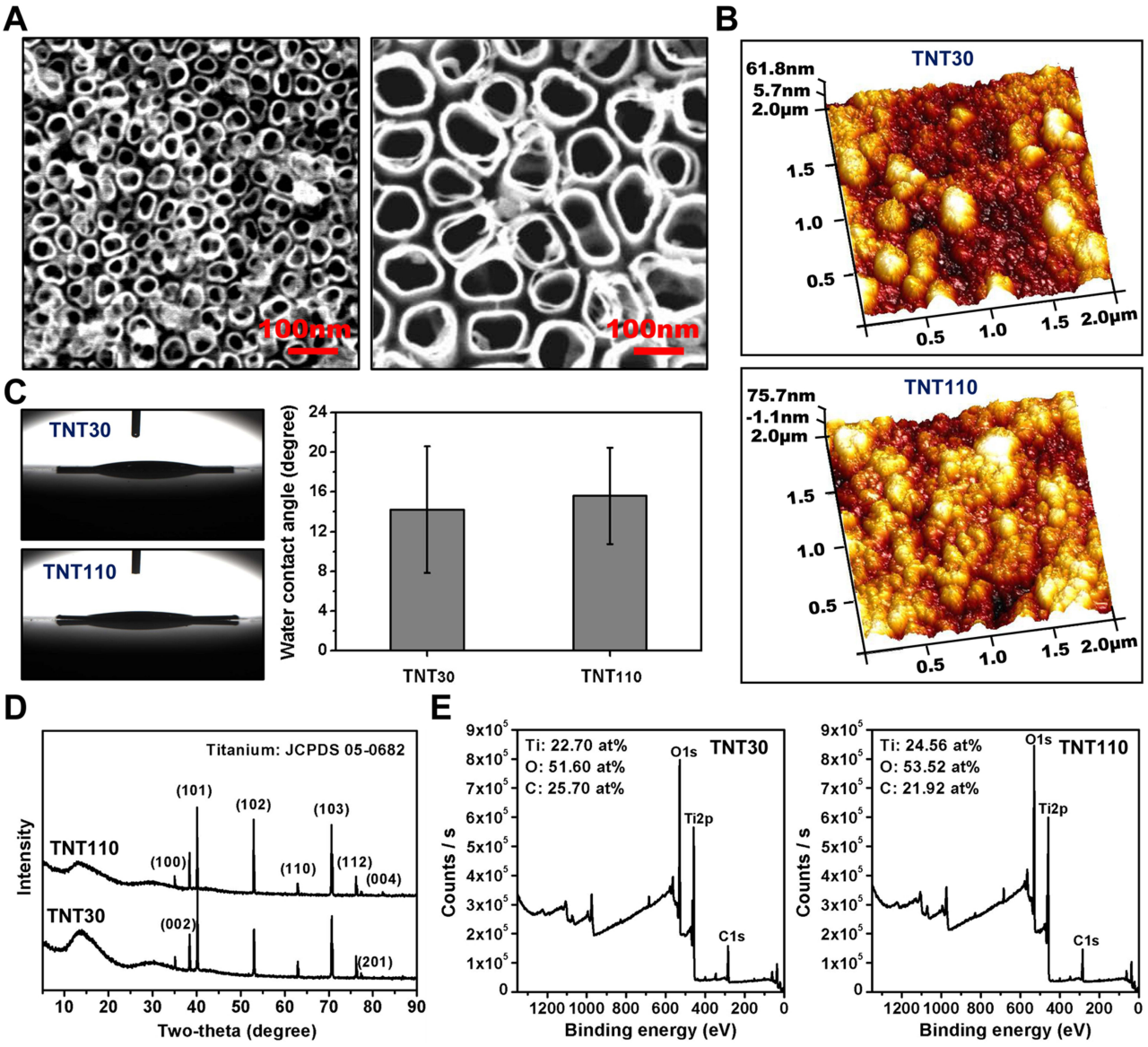

Figure 1 Surface characterization of TNT30 and TNT110. (**A**) Scanning Electron Microscopy (SEM) images; (**B**) Atomic Force Microscopy (AFM) images; (**C**) Water contact angle images and quantitative results; (**D**) X-ray Diffractometer (XRD) analysis; and (**E**) X-ray Photoelectron Spectroscopy (XPS) analysis.

the elemental composition percentages between the two samples. Thus, the TNT30 and TNT110 samples prepared in this study had similar surface physicochemical properties, differing mainly in nanotube diameter.

Osteogenic Performance of Osteoblats on TNTs Under OS Conditions

Figure 2A indicated that under OS, the viability of osteoblasts on the TNT110 surface was significantly higher than that on the TNT30 surface ($*P < 0.05$). The early osteogenic ability of MC3T3-E1 cells was evaluated by measuring ALP activity under OS conditions. Quantitative results shown in Figure 2B demonstrated that ALP activity in TNT110 group was significantly higher than that of the TNT30 ($*P < 0.05$). Late-stage extracellular matrix (ECM) mineralization capacity was assessed via Alizarin Red staining and quantitative analysis. The results (Figure 2C) also indicated that in an OS environment, the mineralization ability of osteoblasts on the TNT110 surface was superior to that on the TNT30 ($*P < 0.05$). Additionally, staining results (Figure S1) displayed a similar trend, with a greater number of mineralized nodules observed on the TNT110 surface compared to TNT30.

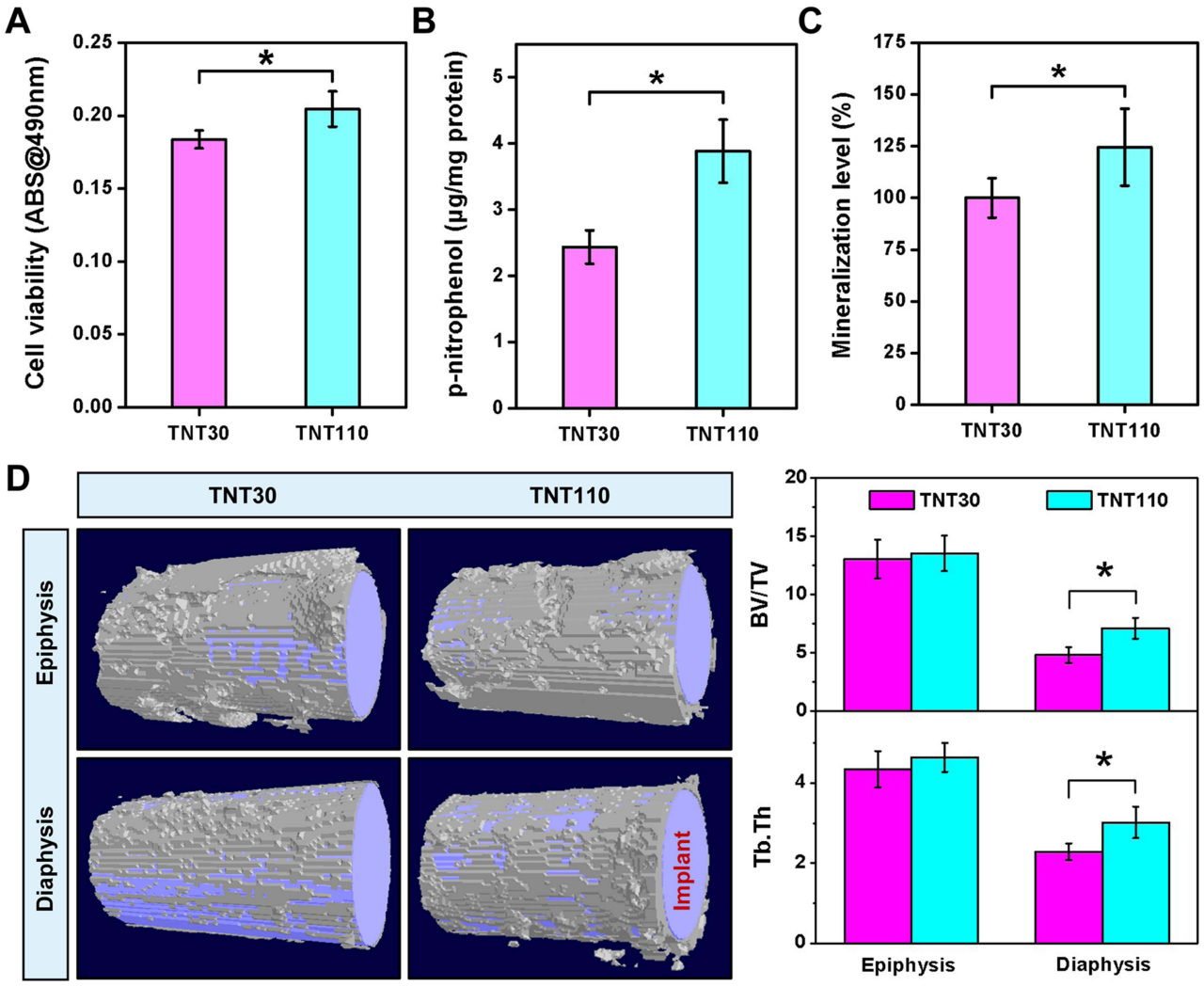

Figure 2 Osteogenic ability of TNT30 and TNT110 under oxidative stress conditions. (**A**) Cell viability of MC3T3-E1 cells; (**B**) Quantitative results of alkaline phosphatase (ALP) activity; (**C**) Quantitative results of mineralization; and (**D**) Representative micro-CT scan images of newly formed bone tissue around titanium implants in aged SD rats, along with quantitative statistics of bone volume/total volume ratio (BV/TV), and trabecular spacing of bone (Tb.Th), *$P < 0.05$.

Localized Osteogenic Capacity of TNT Implants in Aged SD Rats

New bone formation around two groups of titanium implants in aged SD rats was observed using Micro-CT, with the results shown in Figure 2D. Two specific regions (epiphysis and diaphysis) were selected to evaluate bone formation in vivo. The purple area represents the implant, and the white tissue represents the newly formed bone tissue. The new bone volume (BV/TV) and trabecular spacing (Tb.Th) around the implant in the TNT110 group were significantly higher (*$P < 0.05$) than those in the TNT30 group.

In vitro Transcriptomic Analysis of Osteoblasts Under OS Conditions

Transcriptomic analysis was conducted on osteoblasts cultured on TNT30 and TNT110 surfaces under OS conditions. The principal component analysis (PCA) for RNA sequencing was displayed in Figure S2, indicating partial overlap between the two groups. The heatmap (Figure 3A) and volcano plot (Figure 3B) depicted the DEGs between the two groups. Compared to TNT30, TNT110 group showed 53 genes upregulated and 48 genes downregulated. GSEA of all detected genes (Figure 3C) revealed four upregulated pathways in TNT110 osteoblasts: cell adhesion molecule pathway, ECM receptor interaction pathway, longevity regulation pathway, and protein processing in ER pathway. Five pathways

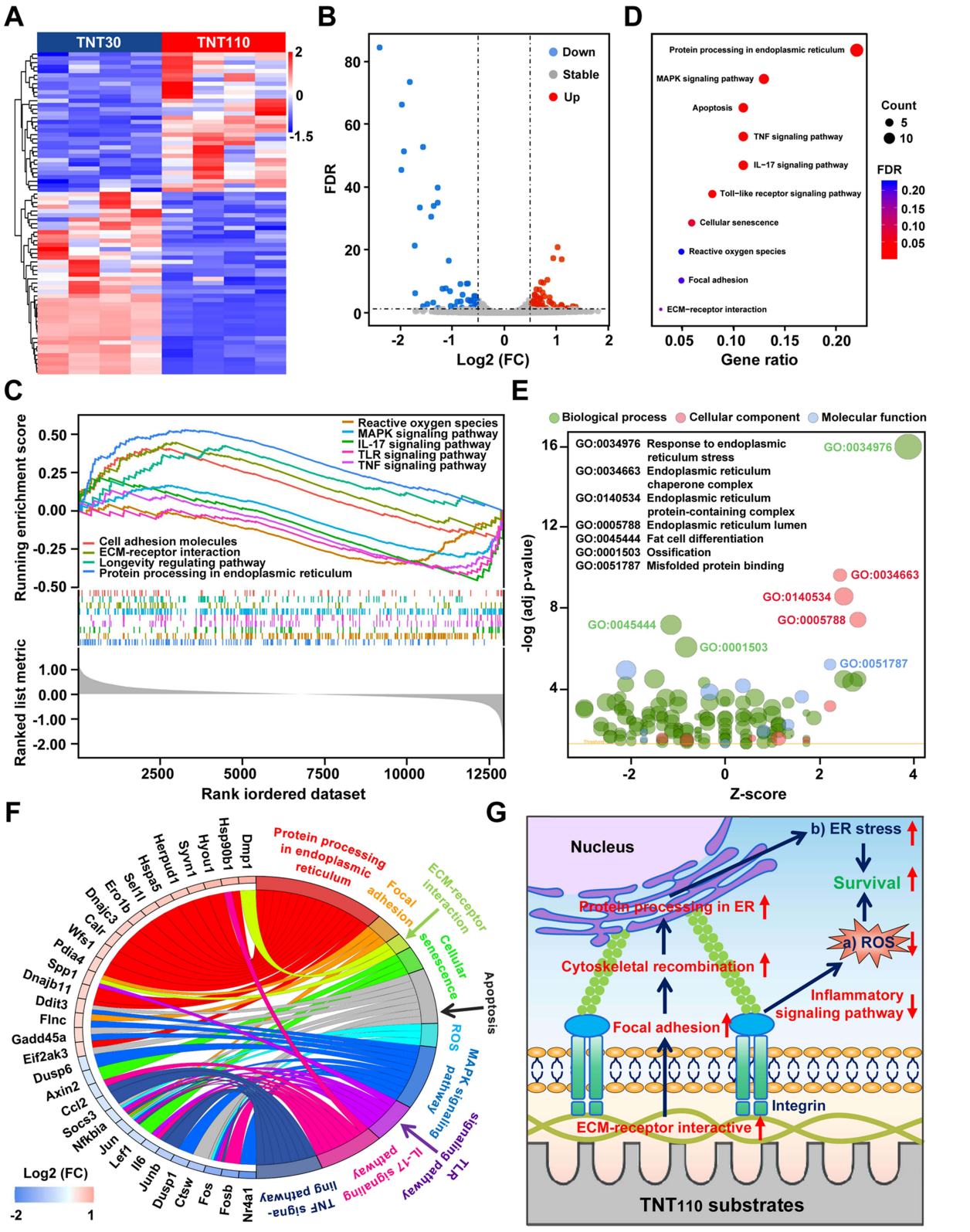

Figure 3 RNA sequencing analysis of MC3T3-E1 cells on TNT30 and TNT110 surfaces in oxidative stress microenvironment. (**A**) Heat map and (**B**) volcano plot of differential genes; (**C**) GSEA analysis of all genes in the two groups; (**D**) KEGG pathway and (**E**) GO enrichment analysis of the differential genes; (**F**) Expression thresholds of the differential genes in the KEGG pathway; and (**G**) Schematic diagram of the mechanism by which TNT110 maintains cell survival.

showed a downward trend, including ROS pathway, MAPK signaling pathway, IL-17 signaling pathway, TLR signaling pathway, and TNF signaling pathway.

KEGG analysis (Figure 3D) was employed to further identify significant pathways, and GO enrichment analysis (Figure 3E) was utilized to elucidate the biological significance of the DEGs. KEGG pathway analysis revealed ten differential signaling pathways: one related to protein processing in ER, one to apoptosis, one to cellular senescence, four to inflammation (MAPK, TNF, IL-17, and Toll-like receptor signaling pathways), one to ROS, and two related to osteoblast growth and differentiation (focal adhesion and ECM receptor interaction pathways). These findings align with GSEA results. Additionally, the GO results confirmed that DEGs were mainly associated with protein processing in the ER and ossification processes. Further analysis of the DEGs in the ten KEGG-enriched pathways revealed that genes related to protein processing in ER (*Hyou1, Herpud1, Syvn1, Sel1l, Calr, Pdia4, Dnajb11, Wfs1, Hspa5, Ddit3, Ero1b, Hsp90b1, Eif2ak3, Dnajc3*), focal adhesion (*Fnc, Spp1*), and ECM receptor interaction (*Dmp1, Spp1*) were upregulated. ROS-related genes (*Fos, Jun, Nfkbia*) were significantly downregulated, while others linked to inflammatory responses or cell survival/apoptosis were mainly downregulated (Figure 3F).

Osteoblast Behaviors on the Surface of TNTs Under OS with/without Serum

Under OS, two time points (30 min and 120 min) were selected to examine the adhesion of osteoblasts on TNT30 and TNT110 surfaces under serum-free and serum-containing conditions. Figure 4A shows a picture of the cell nucleus staining results (the nucleus staining picture of the cells adhered for 30 minutes was selected as a representative), and the quantitative analysis of cell adhesion (Figure 4B) shows that there is no significant difference in cell numbers on TNT30 and TNT110 surfaces was observed after 30 and 120 min in serum-free medium. However, under OS with serum for 30 min, cell adherence to TNT110 was significantly higher than TNT30 ($*P < 0.05$). After 120 min, the adherence on both surfaces increased, with a significant difference still present.

Figure 4A illustrated osteoblast morphology on different sample surfaces under OS with/without serum, while Figure 4C showed the statistical analysis of individual cell spreading areas. Under serum-free conditions, osteoblasts on TNT30 and TNT110 exhibited similar morphology, characterized by wrinkling and cytoplasmic aggregation, with scattered distribution. The statistical analysis revealed no significant difference in cell area between the two groups. In serum-containing conditions, some cells on TNT30 began to spread but lacked intercellular connections. In contrast, on TNT110, most cells were polygonal, some elongated with pseudopodia extending, and visible connections with neighboring cells. The cell area on TNT110 was significantly larger than TNT30 ($*P < 0.05$).

The ROS level in osteoblasts on different sample surfaces under OS, with and without serum, was detected. DCFH-DA staining (Figure 4A) and fluorescence quantification results (Figure 4D) revealed that without serum, there was no significant difference in surface fluorescence intensity between TNT30 and TNT110. However, in serum-containing culture medium, the fluorescence intensity on both TNT30 and TNT110 surfaces significantly reduced compared to the serum-free condition, with TNT110 exhibiting substantially lower ROS level than TNT30 ($*P < 0.05$).

In addition, under OS in serum-free conditions, ER staining (Figure 4A) and quantitative results (Figure 4E) indicated no significant difference in ER Tracker fluorescence intensity on the surface of TNT30 and TNT110. However, in the presence of serum, the fluorescence intensity of ER Tracker in both TNT30 and TNT110 osteoblasts was enhanced compared to serum-free conditions, with TNT110 showing significantly higher fluorescence intensity than TNT30 ($*P < 0.05$).

These findings suggest that the protective effect of TNT110 against OS injury in osteoblasts may be primarily due to the protein coating adsorbed on its surface. Therefore, a more detailed exploration of the composition of surface protein coatings on TNT30 and TNT110 is crucial to understand their potential mechanisms in differentially alleviating cellular OS damage.

Investigation into Osteoblast Adhesion Timing on TNTs Under OS Conditions

In this study, we explored the initial adhesion timing of osteoblasts on nanotube surfaces under OS microenvironment. The cell adhesion results, as illustrated in Figure S3A and B, revealed distinct patterns of adhesion over time. Notably, at the 1 min and 3 min intervals, there was a negligible adhesion of cells on both TNT30 and TNT110 surfaces. However,

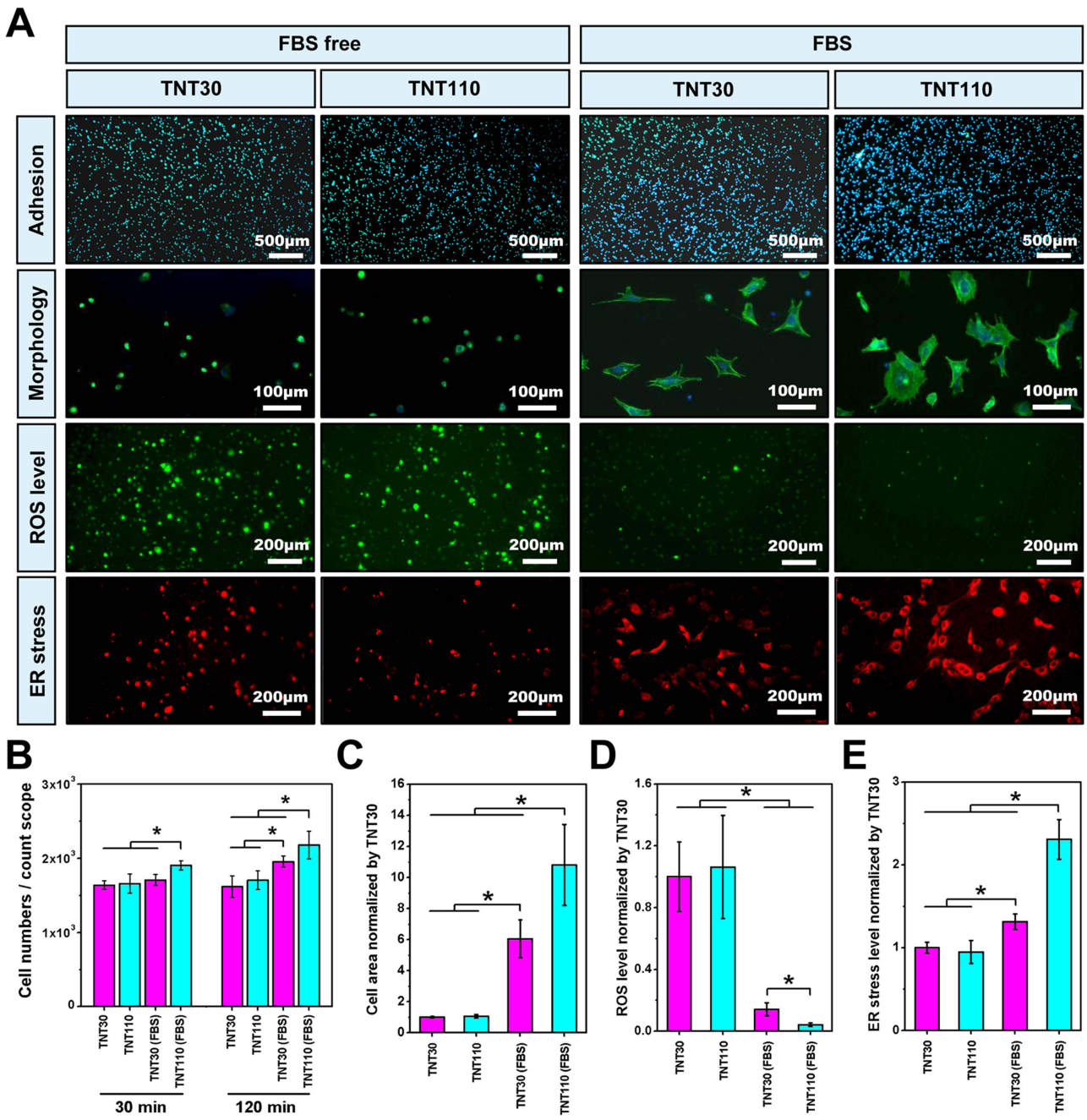

Figure 4 Biological behaviors of MC3T3-E1 cells on TNT30 and TNT110 surface under oxidative stress and with/without serum conditions. (**A**) Early adhesion, morphology, reactive oxygen species (ROS) and endoplasmic reticulum (ER) staining images; Statistical results of cell numbers (**B**), cell diffusion area (**C**), ROS fluorescence intensity (**D**), and ER stress fluorescence intensity (**E**), $^*P < 0.05$.

a significant increase in osteoblast adhesion was observed at 5 min on both TNTs. Moreover, the TNT110 surfaces exhibited a higher number of adherent osteoblasts compared to TNT30 ($^*P < 0.05$). As the incubation time progressed beyond 5 min, we observed a consistent increase in the number of adherent cells on both TNT30 and TNT110 surfaces, following a similar upward trend. Based on these observations, we infer that osteoblasts exhibit substantial adhesion to the nanotube surfaces starting from the 5 min mark. This finding is critical as it establishes a defined "protein pre-adsorption time", which will be instrumental for future research focused on protein adsorption dynamics related to these TNTs.

Investigation of Serum Protein Adsorption on TNTs Under OS

In this section, we examined the adsorption behavior of serum proteins on TNT30 and TNT110. As shown in Figure S4, the total protein content on the surface of TNT110 was significantly higher than on TNT30 (*$P < 0.05$), suggesting that larger-sized TNTs had a greater capacity for protein adsorption under OS. This finding aligned with the trend observed in Figure S3B, where the number of cells adsorbed on the surfaces of these samples after 5 min of incubation also differed.

Further, we conducted a proteomic analysis to understand the differences in the composition of protein layers on different TNTs under OS. After processing the proteomic data and excluding samples with zero protein expression in different groups, the $\log_{10}$(intensity) of all adsorbed proteins were presented in Figure 5B. Notably, the protein component exhibiting the greatest abundance on both TNTs was identified as BSA. This predominance of BSA was likely due to it being the most abundant protein in plasma, thereby increasing its availability for adsorption on the material's surface under OS conditions. The volcano plot in Figure 5C revealed that compared to TNT30, the protein layer on TNT110 featured an increase in the adsorption of six proteins [FN, Complement C3 (C3), Vitronectin (VTN), Serpin family G member 1 (SERPING1), Complement C4A (C4A), Cytokeratin-1 (CK1)] and a decrease in three others [Fetuin B (FETUB), Alpha-2-HS-glycoprotein (AHSG), Complement factor B (CFB)]. Notably, FN, an extracellular matrix protein essential for cell adhesion, exhibited the most significant upregulation in the TNT110 group.

Utilizing the STRING database (https://www.string-db.org/), we further analyzed the Protein-Protein Interaction Networks (PPI) among the detected proteins, displayed in Figure 5D. Four proteins (BSA, VTN, SERPING1, THBS1) interact with FN. BSA, abundant in plasma and known for its antioxidant capacity, along with the other three proteins, which are primarily related to the coagulation process, were highlighted. This suggests that the competitive adsorption of FN and BSA may be pivotal to the enhanced antioxidant stress performance of TNT110, making them key focuses for subsequent research.

To validate the differential adsorption capacities of FN and BSA on various nanotube surfaces under OS, we performed WB experiments. The results (Figure 5E) showed that FN adsorption on TNT110 was significantly higher than on TNT30, whereas BSA adsorption did not significantly differ between the two surfaces. This finding corroborated our proteomic analysis observations.

Characterization and Cellular Responses of TNTs Pre-Adsorbed with Different Proteins Under OS Conditions

Building on the proteomic results previously discussed, we pre-adsorbed TNT30 and TNT110 with solutions of FBS, FN, BSA, and FN/BSA. SEM images (Figure 6A) revealed distinct protein deposition patterns (Figure 6B): on TNT30 surface, proteins directly deposited at the tube mouth, forming layered structures; in contrast, on TNT110 surface, proteins first adsorbed onto the tube wall, accumulating into granular aggregates over time. Interestingly, the lower concentration of FN in the pre-adsorption solution resulted in significantly reduced protein distribution on TNT30(FN) and TNT110(FN) samples, as compared to other groups. This was further substantiated by XPS results (Figure S5), where the elemental nitrogen (N) content on the material's surface served as an indirect indicator of protein adsorption capacity. The N content for both TNT30(FN) and TNT110(FN) was markedly lower than that of other groups. The specific N content of each group was as follows: TNT30(FBS) 15.43 at%, TNT30(FN) 2.08 at%, TNT30(BSA) 13.76 at %, TNT30(FN/BSA) 13.47 at%, TNT110(FBS) 10.12 at%, TNT110(FN) 1.66 at%, TNT110(BSA) 9.15 at%, TNT110 (FN/BSA) 12.04 at%.

Additionally, water contact angle measurements (Figure 6C) indicate an increase in surface hydrophobicity for each sample post protein pre-adsorption. The smallest increase was observed in the TNT30(FN) and TNT110(FN) groups, likely due to the low concentration of FN pre-adsorption. For TNT30, FBS pre-adsorption led to the most pronounced hydrophobicity increase, whereas for TNT110, it was the FN/BSA pre-adsorption group that showed the most significant increase. The specific WCA values were as follows: TNT30(FBS) 54.33±9.23°, TNT30(FN) 19.42±7.82°, TNT30(BSA) 46.56±8.47°, TNT30(FN/BSA) 49.33±6.82°, TNT110(FBS) 52.30±4.32°, TNT110(FN) 17.46±9.28°, TNT110(BSA) 51.88±9.86°, TNT110(FN/BSA) 53.61±5.77°.

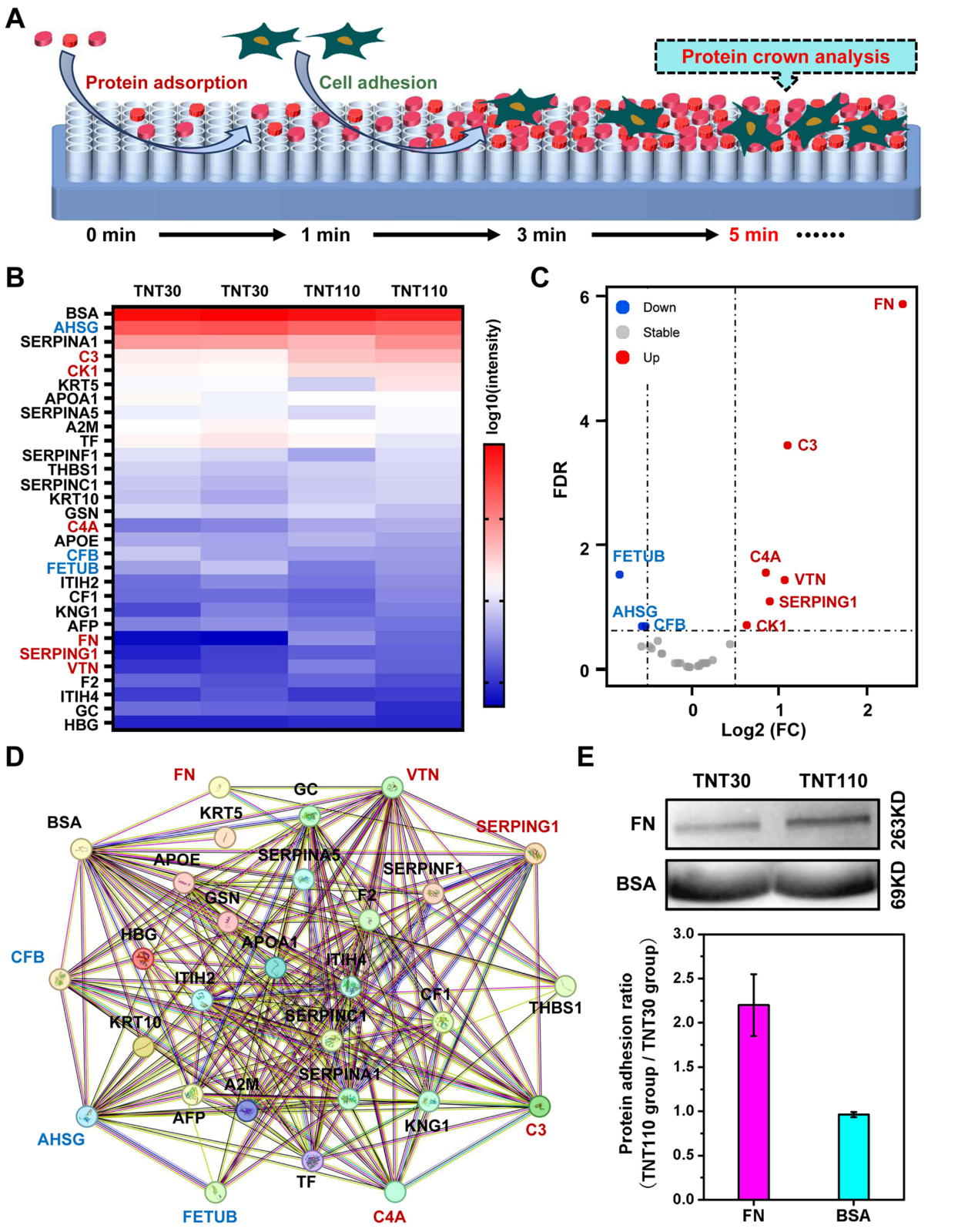

Figure 5 Proteomic analysis of TNT30 and TNT110 groups after serum adsorption under oxidative stress conditions. (**A**) Schematic diagram of protein adsorption and cell adhesion processes; (**B**) Heat map and (**C**) volcano plot of differential proteins on the surface of the two samples; (**D**) Interaction analysis of proteins; and (**E**) Western blotting images of the adsorbed FN and BSA on the sample surfaces, accompanied by statistical graphs of the band gray values.

https://doi.org/10.2147/IJN.S488154 DovePress

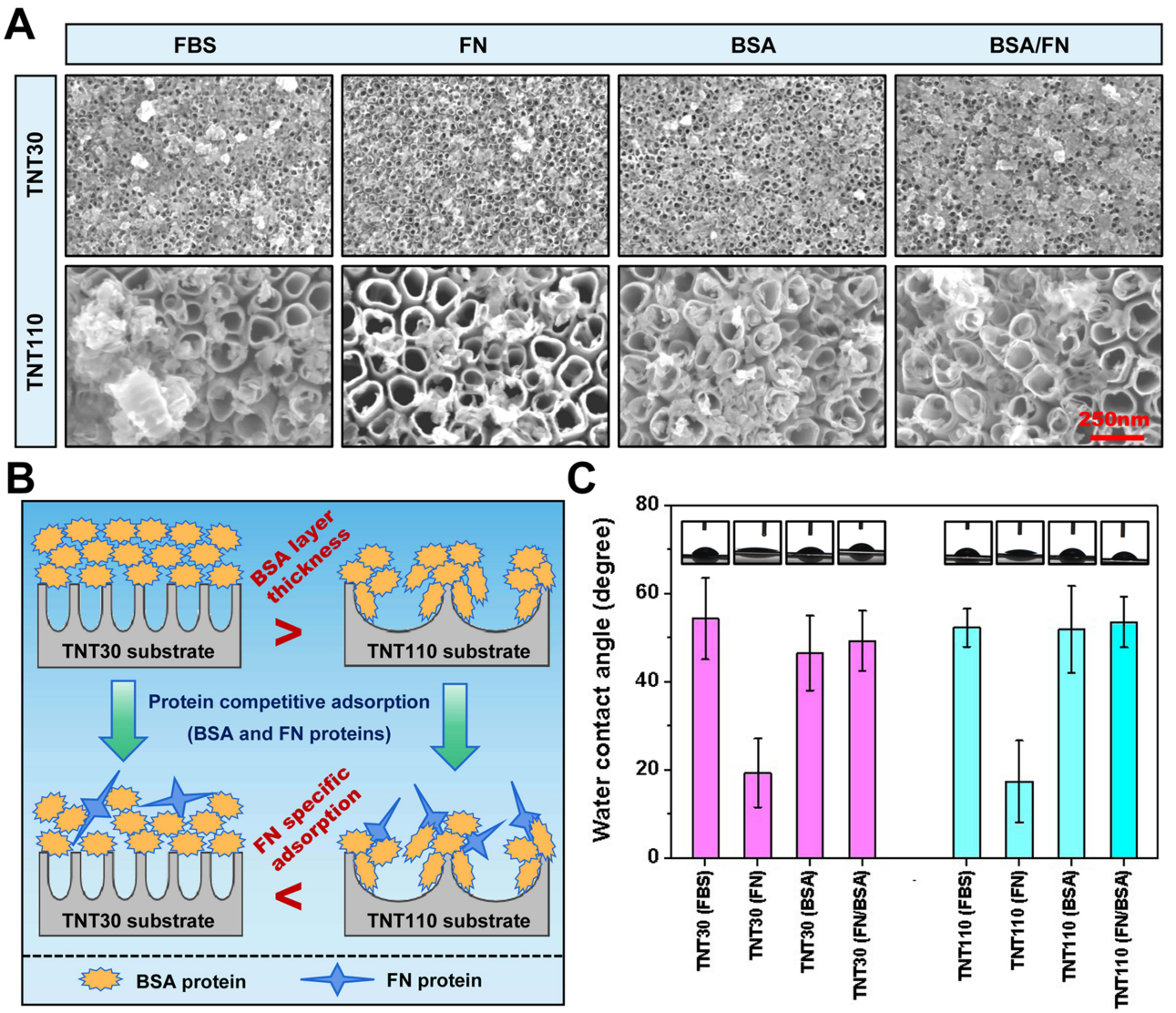

Figure 6 Surface characterization of TNT30 and TNT110 samples after preadsorption treatment with FBS, FN, BSA and FN/BSA protein solutions containing 300 μM H_2O_2. (**A**) SEM images; (**B**) Schematic representation of the competitive adsorption of FN and BSA; (**C**) Water contact angle images and their quantitative analysis.

Subsequently, we assessed osteoblast adhesion and viability on the various sample surfaces under OS and serum-free culture conditions. Nuclear staining images (Figure 7A) and cell count statistics (Figure 7B) revealed that after 30 and 120 min of culture, the TNT110(FN/BSA) exhibited a significant increase in osteoblast adhesion compared to TNT110 (FN) and TNT110(BSA) groups. This increase was statistically significant (*$P < 0.05$) and comparable to the TNT110 (FBS) group at 120 min. In contrast, this trend was not pronounced among TNT30(FBS), TNT30(FN), TNT30(BSA), and TNT30(FN/BSA) groups. Cell viability results (Figure 7C) indicated distinct responses to different pre-adsorption treatments after 6 and 24 h of cultivation. Initially, at 6 h, both TNT30 and TNT110 samples pre-treated with FN or BSA alone [TNT30(FN), TNT30(BSA), TNT110(FN), and TNT110(BSA)] demonstrated a decrease in osteoblast activity compared to the FBS pre-adsorption groups [TNT30(FBS) and TNT110(FBS)]. Conversely, TNT30(FN/BSA) and TNT110(FN/BSA) groups showed an increase in cell activity, aligning with the results observed in both FBS groups. This trend continued at 24 h, with the cell viability on TNT110 surface being notably higher in the FN/BSA group [TNT110(FN/BSA)] than in other groups, and the difference was statistically significant (*$P < 0.05$).

Under serum-free culture conditions in OS, we also investigated osteoblast spreading and intracellular ROS expression following protein pre-adsorption treatment. After 24 h of culture and subsequent staining, the results (Figure 8A)

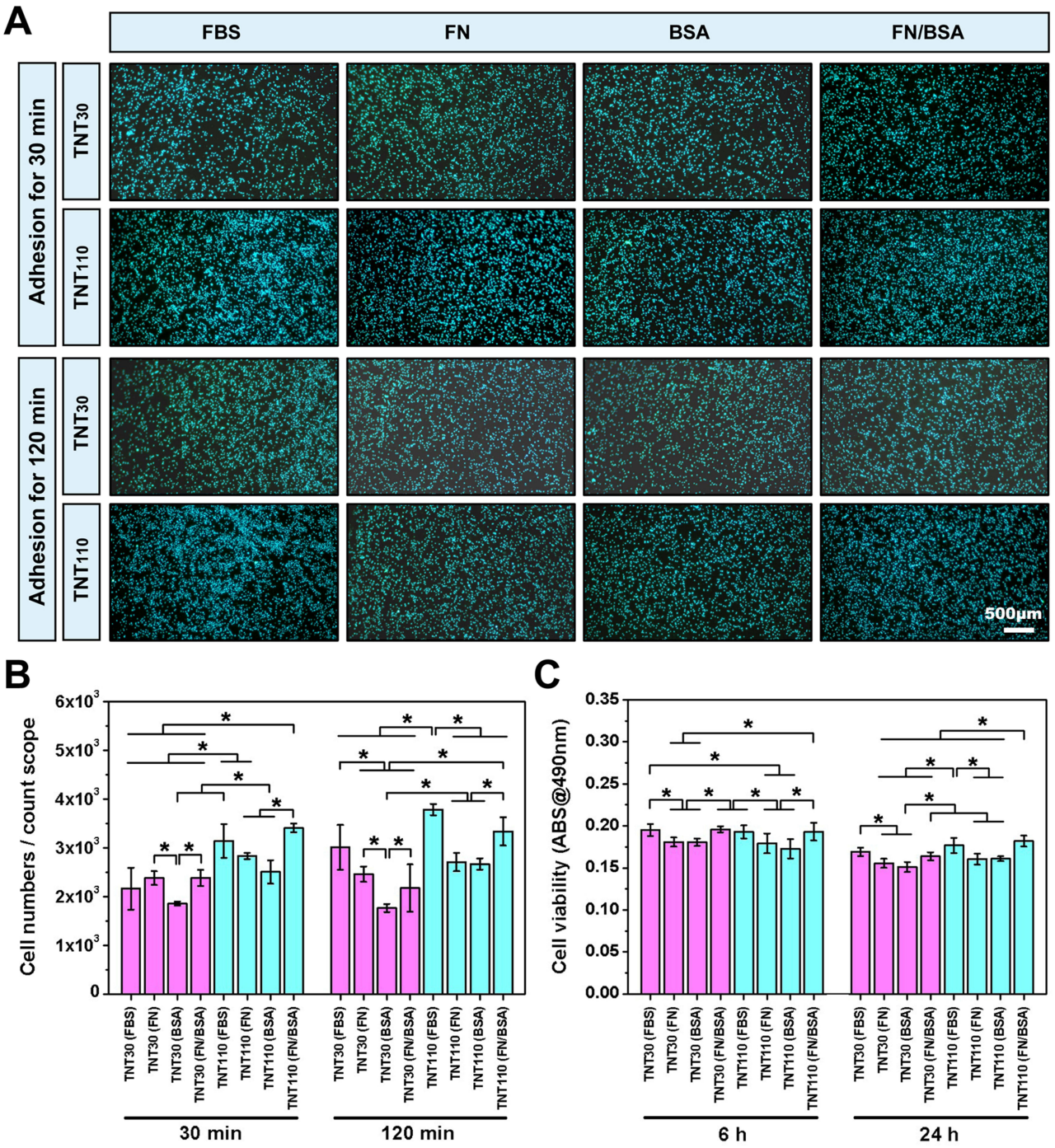

Figure 7 Cell adhesion and viability of MC3T3-E1 cells on TNT30 and TNT110 surfaces after protein pre-adsorption under oxidative stress conditions. (**A**) Nuclear staining images after 30 and 120 min of incubation; and (**B**) quantitative results of cellular adhesion; (**C**) Results of the MTT assay indicating cell viability, *$P < 0.05$.

revealed notable differences in cell distribution and morphology. Compared to the TNT30(FBS) and TNT110(FBS) groups, osteoblasts on TNT30(FN), TNT30(BSA), TNT110(FN), and TNT110(BSA) surfaces were more dispersed, typically forming circular shapes. However, after pre-adsorption with the FN/BSA mixed protein solution, the majority of osteoblasts on the surface of TNT110(FN/BSA) samples displayed polygonal layouts with extensions connecting to adjacent cells, similar to the TNT110(FBS) group. The spreading area of individual cells in this group was comparable to that observed in the TNT110(FBS) group. In contrast, the TNT30(FN/BSA) group did not exhibit significant

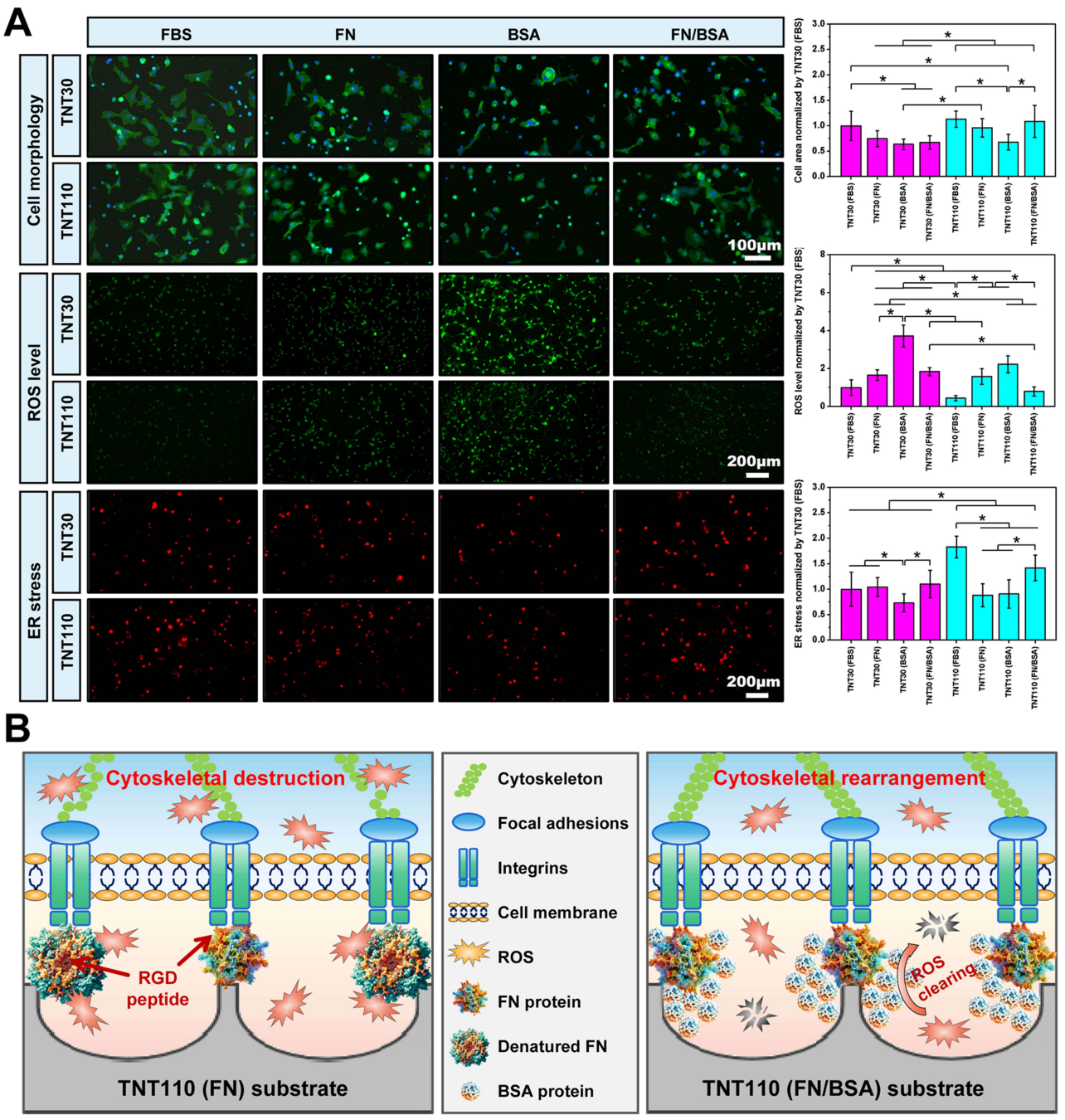

Figure 8 Cell behaviors of MC3T3-E1 cells on TNT30 and TNT110 surfaces after protein pre-adsorption under oxidative stress conditions. (**A**) Cell morphology, ROS, ER staining images along with their corresponding quantitative results, **P* < 0.05; (**B**) Schematic diagram illustrating the mechanism by which BSA and FN exert synergistic effects on the surface of TNT110.

improvements in surface cell spreading. Furthermore, DCFH-DA fluorescence staining was employed to evaluate endogenous ROS expression, with the results depicted in Figure 8A. Compared to the FBS pre-adsorption groups, both TNT30 and TNT110 samples exhibited higher surface fluorescence intensity following pre-adsorption treatment with BSA or FN alone. Notably, the fluorescence intensity in the TNT30(FN) and TNT110(FN) groups was lower than in the TNT30(BSA) and TNT110(BSA) groups. When pre-treated with a mixed FN/BSA protein solution, the surface fluorescence intensity of TNT30(FN/BSA) was similar to the TNT30(FN) group, whereas TNT110(FN/BSA) showed

significantly lower fluorescence intensity compared to the BSA and FN pre-adsorption groups (*$P < 0.05$), aligning closely with the FBS pre-treated group.

Additionally, ER Tracker Red fluorescent probe staining was used to investigate the activity of ER in osteoblasts, with results also presented in Figure 8A. Relative to the FBS pre-adsorption groups, the fluorescence intensity of ER staining on the surface of TNT110 (FN) and TNT110 (BSA) was markedly weaker after pre-treatment with FN or BSA alone. However, this trend was reversed in the TNT110(FN/BSA) group, where the fluorescence intensity of ER staining was significantly enhanced, surpassing that of both TNT30(FN/BSA) and TNT30(FBS) groups. For TNT30 samples, post FN/BSA mixed protein pre-adsorption, the surface fluorescence intensity of TNT30(FN/BSA) was stronger than the TNT30 (BSA) group, but did not show a significant difference from the TNT30(FN) group.

Discussion

TNTs have become one of the most commonly used nanomodification techniques for Ti implant surfaces due to their good biological compatibility, mechanical properties, and corrosion resistance.[11,12] Additionally, the size of the nanotubes influences their biological activity. In normal microenvironments, smaller TNTs are known to promote osteoblast adhesion and proliferation, whereas larger TNTs are more favorable for osteogenic differentiation.[13] However, under in vitro OS conditions, the biological activity of small-sized TNTs (TNT30) is considerably inhibited. In contrast, larger nanotubes (TNT110) can sustain osteoblast proliferation and differentiation by influencing cell morphology and ITGα5β1 expression.[16] Given that the surface physicochemical properties of TNT30 and TNT110 are nearly identical, aside from the difference in tube diameter (Figure 1), the greater resistance of osteoblasts on TNT110 to OS is attributed to the larger nanotube diameter. However, the precise mechanisms underlying this enhanced stress resistance remain unclear. To further explore this, the present study examined the biological behaviors of osteoblasts on TNT30 and TNT110 under OS both in vitro and in vivo, using proteomic and RNA sequencing analyses to investigate potential mechanisms. In addition, to model oxidative damage, we developed an in vitro osteoblast OS injury model by supplementing the cell culture medium with 300 μM H_2O_2.[16] Common approaches for inducing OS in cellular models include H_2O_2 induction, chemical agents, hypoxia-reoxygenation, and so on.[24,25] Among these, the H_2O_2-induced model is widely used to simulate OS damage related to aging due to its simplicity and strong controllability.[26,27] By adding an appropriate amount of H_2O_2 to the culture medium, intracellular ROS levels can be rapidly elevated, triggering OS responses.[16,27] This method effectively mimics the mechanisms of cellular damage caused by free radical accumulation during aging and has broad applicability across various cell types.

There was no significant difference in the biological activity of TNT30 and TNT110 surface osteoblasts in the OS microenvironment under serum-free culture conditions. In contrast, in the presence of serum, osteoblasts on the surface of TNT110 showed stronger early adhesion, better cell spreading area, and significantly lower ROS expression compared to TNT30 (Figure 4A-E). This result suggests that serum proteins play a key role in mediating the oxidative damage mitigation ability of TNT110. Protein adsorption from blood and other tissue fluids is the first event that occurs at the biomaterial-tissue interface after implantation of biomaterials in vivo, rapidly forming a protein crown on the surface of the material.[17,28] Biomaterial surface properties can indirectly influence subsequent cell behavior (eg adhesion, migration, growth, and differentiation) by affecting the type, amount, and conformation of adsorbed proteins.[19] In addition, cell-biomaterial surface interactions are mediated by multiple proteins in the adsorbed protein layer rather than by a single protein,[21] necessitating an in-depth understanding of the surface adsorbed protein layer components and the mechanisms by which they regulate cellular behavior (Figure 5A). We investigated the adsorption of serum proteins on the surface of TNT30 and TNT110 samples under OS conditions using proteomics techniques and found that more total protein was adsorbed from serum on the surface of TNT110 than on the surface of TNT30 (Figure S4). FN, which is associated with cellular adhesion, was adsorbed on the surface of TNT110 at a significantly higher level compared to TNT30 (Figure 5B and C). As an adhesion protein, FN exists in two forms: soluble FN circulating in plasma and insoluble multimeric FN secreted by various cells into the extracellular matrix.[29,30] It can bind to the cell surface transmembrane receptor integrin receptor (ITGα5β1) through its RGD structural domains to transduce the signals from the extracellular matrix into the cell. Integrin will rapidly bind to the actin cytoskeleton, forming focal adhesions and facilitating initial cell adhesion and spreading on the material surface.[31,32] It has been also shown that FN is involved in

the early stages of osteogenesis, and osteoblastic FN plays an important role in the number and function of osteoblasts.[30] FN from the blood circulation can penetrate into the bone matrix, affecting its properties. However, under OS, the structure and function of FN can be altered, and conformational changes in FN will affect its interaction with cell surface receptors.[33,34]

Albumin, the most abundant protein in plasma, can act as a carrier for endogenous or exogenous substances, delivering them to the target sites.[35] Meanwhile, albumin contributes significantly to the antioxidant capacity of human plasma and serves as an important extracellular antioxidant.[36,37] Our study on the differential protein interactions on the surface of TNT30 and TNT110 revealed an interaction between FN and BSA (Figure 5D). Therefore, we selected these two proteins for further investigation. We found that in the TNT110 group, compared to the groups treated with either FN or BSA pre-adsorption alone, the mixed protein solution of FN/BSA significantly increased cell viability, adhesion, and spreading area of MC3T3-E1 cells on the sample surface. Additionally, it significantly decreased the expression of endogenous ROS, closely resembling the effects observed in the group treated with FBS pre-adsorption (Figure 8A). However, this phenomenon was not evident on the TNT30 sample surface. This suggests that FN and BSA play a synergistic role on the surface of TNT110 samples. Based on this, we hypothesized that in the OS microenvironment, FN alone on the surface of TNT110 samples would be susceptible to damage by extracellular ROS, leading to conformational changes and impaired function. As a result, under OS conditions, FN may struggle to provide the full antioxidant protection associated with TNT110 when used in isolation. While BSA may not be the direct contributor to TNT110's oxidative resistance, it likely plays an essential role in enhancing the protective effects of FN against oxidative damage in osteoblasts. BSA, known as the primary antioxidant protein in plasma, is a vital component of the body's antioxidant defense system.[35–37] Therefore, in an OS environment, BSA within the protein layer may shield FN from oxidative damage by scavenging extracellular ROS, as illustrated in Figure 8B. This protective mechanism enables FN to retain its biological functions, thereby preserving osteoblast activity on the surface of TNT110. In contrast, this protective effect is less evident on TNT30 surfaces. Consequently, we suggest that the differential cellular activity and osteogenic capacity observed in osteoblasts on TNT110 and TNT30 under OS conditions are primarily mediated by the distinct proteins adsorbed on the nanotube surfaces, with FN and BSA playing key roles.

Our study also revealed that the cell viability and osteogenic differentiation of MC3T3-E1 cells on the surface of TNT110 were superior to those on TNT30 in the OS microenvironment. In vivo experiments further demonstrated that TNT110 implants had better osteogenic capacity compared to TNT30. To investigate the underlying molecular mechanisms, we conducted further in vitro transcriptomic assays. GO enrichment analysis and KEGG pathway analysis (Figure 3D-F) showed that the DEGs on the surface of the two samples were mainly related to protein processing and ossification processes in the ER. The protein processing signaling pathways in the ER on the surface of TNT110 were up-regulated compared to TNT30 samples, with increased gene expression of the ER membrane protein *Eif2ak3* and the molecular chaperones *Hyou1, Hspa5*, and *Hsp90b1*, among others. Additionally, higher levels of ERS were observed in osteoblasts on the surface of TNT110 compared to TNT30 (Figure 4A). The ER is an essential organelle involved in protein synthesis, folding, and transport.[38] Under conditions such as OS, nutritional deficiencies, and dysregulation of calcium homeostasis, ERS is induced by the accumulation of unfolded and misfolded proteins in the lumen of the ER. In response to early-stage ERS, cells initiate the protective unfolded protein response (UPR) signaling pathway to enhance protein folding capacity and accelerate the degradation of misfolded proteins, thereby alleviating the stress.[39–41] The ERS/UPR response involves multiple regulatory components, including some transmembrane proteins (IRE1α, PERK, and ATF6) and molecular chaperones (Hspa5/GRP78). Under ERS conditions, chaperone molecules dissociate from ER transmembrane proteins, increasing the number of chaperones and protein folding-related molecules and activating the UPR response, ultimately alleviating ERS.[39] In this study, the up-regulation of gene expression of chaperone and protein folding-related molecules (Hyou1, Hspa5, Hsp90b1 and Eif2ak3, etc.) on the surface of TNT110 samples (Figure 3F) indicated that the UPR response had been activated, further controlling the quality of proteins processed in the ER, thus maintaining cell viability.

Transcriptomic analysis also revealed that genes (*Dmp1, Spp1* and *Flnc*) involved in the ECM-receptor interaction signaling and adhesion signaling pathways were significantly up-regulated in osteoblasts on the surface of TNT110 compared to TNT30 under OS conditions (Figure 3D-F). Extracellular matrix proteins adsorbed on the surface of

biomaterials are recognized by a family of integrin receptors on the cell membrane,[32] and when integrins are occupied, they aggregate and trigger other cellular proteins (*eg*, vinculin, focal adhesion kinase, *etc*.) to form an adhesion complex. This complex provides transmembrane connectivity between the extracellular matrix and the F-actin cytoskeleton, and triggers subsequent cellular behaviours such as cell adhesion, spreading, and osteogenic differentiation.[42,43] Our study demonstrated that under OS conditions, more FN protein was adsorbed on the surface of TNT110 samples than on TNT30 (Figure 5B and C). Previous findings have shown that the adsorbed FN could bind to integrin receptors on the surface of osteoblasts, promoting the assembly of integrin α5β1 into focal adhesion and regulating the rearrangement of actin filaments to maintain osteoblasts survival.[16] The transcription of genes *(Fos, Fosb, Jun, Nfkbia, Il6*) associated with multiple inflammatory pathways (MAPK signalling pathway, TNF signalling pathway, IL-17 signalling pathway, and Toll-like receptor signalling pathway) on the surface of TNT110 was down-regulated (Figure 3D-F), and this down-regulation inhibited the inflammatory response and the activation of apoptotic pathways.[44,45] The transcript levels of genes in the ROS pathway on the surface of TNT110 were also decreased, in which the down-regulation of *Nfkbia* could inhibit the activation of the NF-κB pathway to induce the expression of antioxidant genes, down-regulate intracellular ROS, and help the cells to mitigate oxidative damage.[46] In addition, although the activation of signaling pathways directly related to osteogenesis was not detected in the transcriptomics results, the transcription of the mineralisation-related gene *Spp1* was up-regulated, suggesting that the early osteogenic behaviors of osteoblasts have been activated.[47] Moreover, mild ERS level has been also shown to promote osteogenic differentiation of osteoblasts.[48,49]

Based on the above description, we further summarized the biological behaviors of osteoblasts on TNTs surface under OS conditions and their underlying molecular mechanisms, as shown in Figure 3G. Osteoblasts on TNT110 surfaces show enhanced survival compared to TNT30. We surmise that there are two protective mechanisms against oxidative damage in TNT110 group: firstly, surface-adsorbed proteins may activate ECM-receptor interactions, facilitating the formation of adhesion patches, cytoskeletal rearrangement, and ER-mediated protein synthesis; secondly, the osteoblasts mitigate oxidative damage by downregulating inflammation pathways and reducing ROS expression. While we have confirmed the importance of the synergistic effects of FN and BSA in the surface protein corona of TNT110 for antioxidant performance in osteoblasts, the detailed mechanisms of their interaction remain unclear. Future research will explore these interactions more extensively to fully elucidate the protective effects.

Conclusion

This study reveals that MC3T3-E1 cells on TNT110 surfaces display improved survival and osteogenic capability under OS compared to TNT30. Transcriptomic analyses show TNT110 enhances cell survival, adhesion, and spreading by influencing inflammation, ER processing, ROS, focal adhesion, and ECM-receptor pathways. Proteomic data highlighted increased FN adsorption on TNT110, with FN/BSA pre-adsorption markedly boosting osteoblast functions, especially on TNT110. It implies BSA preserves FN, promoting its osteoblast recognition, thus attenuating oxidative damage and preserving cell functionality. These findings aid in developing Ti implants for elderly patients, enhancing early osseointegration by reducing oxidative damage.

Data Sharing Statement

The dataset used and/or analysed during the current study are available from the corresponding author (Xinkun Shen) on reasonable request.

Ethics Declarations

The authors declare no interest conflict. They have no known competing financial interests or personal relationships that could have appeared to influence the work reported in this paper.

Ethics Approval and Consent to Participate

All animal experiments were approved and passed by the Ethics Committee of Ruian People's Hospital (Approval number: SYSQ-2023-022), which were strictly following the ethical standards laid down in the 1964 Declaration of Helsinki and its later amendments.

Acknowledgments

Yun Xiang and Dini Lin contributed equally to this work and share first authorship.

Funding

This work was funded by National Natural Science Foundation of China (82171004), Zhejiang Provincial Science and Technology Project for Public Welfare (LQ23H140001), Wenzhou Municipal Science and Technology Project for Public Welfare (Y20220922), and Wenzhou Medical University Basic Scientific Research Operating Expenses (KYYW202230).

Disclosure

The authors report no conflicts of interest in this work.

References

1. Sun XD, Liu TT, Wang QQ, Zhang J, Cao MS. Surface modification and functionalities for titanium dental implants. *ACS Biomater Sci Eng*. 2023;9(8):4442–4461. doi:10.1021/acsbiomaterials.3c00183
2. Bryant SR, Zarb GA. Crestal bone loss proximal to oral implants in older and younger adults. *J Prosthet Dent*. 2003;89(6):589–597. doi:10.1016/S0022-3913(03)00199-9
3. Sreedhar A, Aguilera-Aguirre L, Singh KK. Mitochondria in skin health, aging, and disease. *Cell Death Dis*. 2020;11(6):444. doi:10.1038/s41419-020-2649-z
4. Bai L, Chen PR, Zhao Y, et al. A micro/nano-biomimetic coating on titanium orchestrates osteo/angio-genesis and osteoimmunomodulation for advanced osseointegration. *Biomaterials*. 2021;278:121162. doi:10.1016/j.biomaterials.2021.121162
5. Han J, Wang Y, Zhou H, Zhang Y, Wan D. Cd137 regulates bone loss via the p53 wnt/β-catenin signaling pathways in aged mice. *Front Endocrinol*. 2022;13:922501. doi:10.3389/fendo.2022.922501
6. Hajam YA, Rani R, Ganie SY, et al. Oxidative stress in human pathology and aging: molecular mechanisms and perspectives. *Cells*. 2022;11(3):552. doi:10.3390/cells11030552
7. Wang YF, Chang YY, Zhang XM, et al. Salidroside protects against osteoporosis in ovariectomized rats by inhibiting oxidative stress and promoting osteogenesis via nrf2 activation. *Phytomedicine*. 2022;99:154020. doi:10.1016/j.phymed.2022.154020
8. Hong GJ, Chen ZQ, Han XR, et al. A novel rankl-targeted flavonoid glycoside prevents osteoporosis through inhibiting nfatc1 and reactive oxygen species. *Clin Transl Med*. 2021;11(5):e392. doi:10.1002/ctm2.392
9. Zhang J, Zhao C, Sheng R, Lin K, Wang X, Zhang S. Construction of a hierarchical micro-/submicro-/nanostructured 3D-printed Ti6Al4V surface feature to promote osteogenesis: involvement of Sema7A through the ITGB1/FAK/ERK signaling pathway. *ACS Appl Mater Interfaces*. 2022;14(27):30571–30581. doi:10.1021/acsami.2c06454
10. Joshi MU, Kulkarni SP, Choppadandi M, Keerthana M, Kapusetti G. Current state of art smart coatings for orthopedic implants: a comprehensive review. *Smart Mater Med*. 2023;4:661–679. doi:10.1016/j.smaim.2023.06.005
11. Gulati K, Chopra D, Kocak-Oztug NA, Verron E. Fit and forget: the future of dental implant therapy via nanotechnology. *Adv Drug Deliv Rev*. 2023;199:114900. doi:10.1016/j.addr.2023.114900
12. Oh S, Brammer KS, Li YSJ, et al. Stem cell fate dictated solely by altered nanotube dimension. *Proc Natl Acad Sci*. 2009;106(7):2130–2135. doi:10.1073/pnas.0813200106
13. Lv LW, Liu YS, Zhang P, et al. The nanoscale geometry of TiO_2 nanotubes influences the osteogenic differentiation of human adipose-derived stem cells by modulating H3K4 trimethylation. *Biomaterials*. 2015;39:193–205. doi:10.1016/j.biomaterials.2014.11.002
14. Huang J, Li R, Yan J, et al. Bioadaptation of implants to in vitro and in vivo oxidative stress pathological conditions via nanotopography-induced foxo1 signaling pathways to enhance osteoimmunal regeneration. *Bioact Mater*. 2021;6(10):3164–3176.
15. Yang J, Zhang H, Chan SM, et al. TiO_2 nanotubes alleviate diabetes-induced osteogenetic inhibition. *Int J Nanomed*. 2020;15:3523–3537. doi:10.2147/IJN.S237008
16. Yu YL, Shen XK, Luo Z, et al. Osteogenesis potential of different titania nanotubes in oxidative stress microenvironment. *Biomaterials*. 2018;167:44–57. doi:10.1016/j.biomaterials.2018.03.024
17. Wu S, Zhang DT, Bai J, et al. Adsorption of serum proteins on titania nanotubes and its role on regulating adhesion and migration of mesenchymal stem cells. *J Biomed Mater Res A*. 2020;108(11):2305–2318. doi:10.1002/jbm.a.36987
18. Zhao Q, Zhao Z, Zhang J, et al. Fn-hmgb1 adsorption behavior initiates early immune recognition and subsequent osteoinduction of biomaterials. *Adv Healthc Mater*. 2024;13(2):e2301808. doi:10.1002/adhm.202301808
19. Barberi J, Ferraris S, Giovannozzi AM, et al. Advanced characterization of albumin adsorption on a chemically treated surface for osseointegration: an innovative experimental approach. *Mater Design*. 2022;218:110702.
20. Firkowska-Boden I, Zhang XY, Jandt KD. Controlling protein adsorption through nanostructured polymeric surfaces. *Adv Healthc Mater*. 2018;7(1):1700995. doi:10.1002/adhm.201700995
21. Othman Z, Pastor BC, van Rijt S, Habibovic P. Understanding interactions between biomaterials and biological systems using proteomics. *Biomaterials*. 2018;167:191–204. doi:10.1016/j.biomaterials.2018.03.020
22. Luo JJ, Walker M, Xiao YB, Donnelly H, Dalby MJ, Salmeron-Sanchez M. The influence of nanotopography on cell behaviour through interactions with the extracellular matrix - a review. *Bioact Mater*. 2022;15:145–159.
23. Wu T, Hu E, Xu S, et al. Clusterprofiler 4.0: a universal enrichment tool for interpreting omics data. *Innovation*. 2021;2(3):100141.
24. Goud AP, Goud PT, Diamond MP, Gonik B, Abu-Soud HM. Reactive oxygen species and oocyte aging: role of superoxide, hydrogen peroxide, and hypochlorous acid. *Free Radic Biol Med*. 2008;44(7):1295–1304. doi:10.1016/j.freeradbiomed.2007.11.014

25. Ebegboni VJ, Dickenson JM, Sivasubramaniam SD. Antioxidative effects of flavonoids and their metabolites against hypoxia/reoxygenation-induced oxidative stress in a human first trimester trophoblast cell line. *Food Chem*. 2019;272:117–125. doi:10.1016/j.foodchem.2018.08.036
26. Miyoshi N, Oubrahim H, Chock PB, Stadtman ER. Age-dependent cell death and the role of ATP in hydrogen peroxide-induced apoptosis and necrosis. *Proc Natl Acad Sci*. 2006;103(6):1727–1731. doi:10.1073/pnas.0510346103
27. Liu X, Xing Y, Yuen M, Yuen T, Yuen H, Peng Q. Anti-aging effect and mechanism of proanthocyanidins extracted from sea buckthorn on hydrogen peroxide-induced aging human skin fibroblasts. *Antioxidants*. 2022;11(10):1900. doi:10.3390/antiox11101900
28. Deng FY, Zhai WY, Yin Y, Peng C, Ning CQ. Advanced protein adsorption properties of a novel silicate-based bioceramic: a proteomic analysis. *Bioact Mater*. 2021;6(1):208–218.
29. Mpoyi EN, Cantini M, Reynolds PM, Gadegaard N, Dalby MJ, Salmerón-Sánchez M. Protein adsorption as a key mediator in the nanotopographical control of cell behavior. *ACS Nano*. 2016;10(7):6638–6647. doi:10.1021/acsnano.6b01649
30. Bentmann A, Kawelke N, Moss D, et al. Circulating fibronectin affects bone matrix, whereas osteoblast fibronectin modulates osteoblast function. *J Bone Miner Res*. 2010;25(4):706–715. doi:10.1359/jbmr.091011
31. Cao K, Wang Z, Sun X, et al. Scaffold adhering to peptide-based biomimetic extracellular matrix composite nanobioglass promotes the proliferation and migration of skin fibroblasts through the GSK-3β/β-catenin signaling axis. *Int J Nanomed*. 2024;19:2957–2972. doi:10.2147/IJN.S449385
32. González-García C, Sousa SR, Moratal D, Rico P, Salmerón-Sánchez M. Effect of nanoscale topography on fibronectin adsorption, focal adhesion size and matrix organisation. *Colloids Surf B Biointerfaces*. 2010;77(2):181–190. doi:10.1016/j.colsurfb.2010.01.021
33. He J, Becares ER, Thulstrup PW, et al. Peroxynitrous acid (onooh) modifies the structure of anastellin and influences its capacity to polymerize fibronectin. *Redox Biol*. 2020;36:101631. doi:10.1016/j.redox.2020.101631
34. Suzuki H, Hayakawa M, Kobayashi K, Takiguchi H, Abiko Y. H_2O_2-derived free radicals treated fibronectin substratum reduces the bone nodule formation of rat calvarial osteoblast. *Mech Ageing Dev*. 1997;98(2):113–125. doi:10.1016/S0047-6374(97)00077-8
35. Belinskaia DA, Voronina PA, Shmurak VI, Jenkins RO, Goncharov NV. Serum albumin in health and disease: esterase, antioxidant, transporting and signaling properties. *Int J Mol Sci*. 2021;22(19):10318.
36. Gao HH, Hou NC, Gao X, et al. Interaction between Chinese quince fruit proanthocyanidins and bovine serum albumin: antioxidant activity, thermal stability and heterocyclic amine inhibition. *Int J Biol Macromol*. 2023;238:124046. doi:10.1016/j.ijbiomac.2023.124046
37. Anraku M, Shintomo R, Taguchi K, et al. Amino acids of importance for the antioxidant activity of human serum albumin as revealed by recombinant mutants and genetic variants. *Life Sci*. 2015;134:36–41. doi:10.1016/j.lfs.2015.05.010
38. Nam SM, Jeon YJ. Proteostasis in the endoplasmic reticulum: road to cure. *Cancers*. 2019;11(11):1793.
39. Wu JS, Li WM, Chen YN, Zhao Q, Chen QF. Endoplasmic reticulum stress is activated in acute pancreatitis. *J Dig Dis*. 2016;17(5):295–303. doi:10.1111/1751-2980.12347
40. Cai B, Hou M, Zhang S, et al. Dual targeting of endoplasmic reticulum by redox-deubiquitination regulation for cancer therapy. *Int J Nanomed*. 2021;16:5193–5209. doi:10.2147/IJN.S321612
41. Li W, Ca T, Luo CY, et al. Crosstalk between er stress, nlrp3 inflammasome, and inflammation. *Appl Microbiol Biotechnol*. 2020;104(14):6129–6140. doi:10.1007/s00253-020-10614-y
42. Di Cio S, Gautrot JE. Cell sensing of physical properties at the nanoscale: mechanisms and control of cell adhesion and phenotype. *Acta Biomater*. 2016;30:26–48. doi:10.1016/j.actbio.2015.11.027
43. Mishra YG, Manavathi B. Focal adhesion dynamics in cellular function and disease. *Cell Signal*. 2021;85:110046.
44. Liang XP, Liu YJ, Chen L, Chen SY. The natural compound puerarin alleviates inflammation and apoptosis in experimental cell and rat preeclampsia models. *Int Immunopharmacol*. 2021;99:108001. doi:10.1016/j.intimp.2021.108001
45. Wang B, Zheng ZH, Chen L, et al. Transcriptomics reveals key regulatory pathways and genes associated with skin diseases induced by face paint usage. *Sci Total Environ*. 2023;890:164374. doi:10.1016/j.scitotenv.2023.164374
46. Gloire G, Charlier E, Rahmouni S, et al. Restoration of ship-1 activity in human leukemic cells modifies nf-jb activation pathway and cellular survival upon oxidative stress. *Oncogene*. 2023;42(26):2153. doi:10.1038/s41388-023-02697-4
47. Zhang YQ, Zhou L, Fu Q, Liu ZY. ANKRD1 activates the Wnt signaling pathway by modulating CAV3 expression and thus promotes BMSC osteogenic differentiation and bone formation in ovariectomized mice. *Biochim Biophys Acta Mol Basis Dis*. 2023;1869(5):166693. doi:10.1016/j.bbadis.2023.166693
48. Shi MQ, Song W, Han TX, et al. Role of the unfolded protein response in topography-induced osteogenic differentiation in rat bone marrow mesenchymal stem cells. *Acta Biomater*. 2017;54:175–185. doi:10.1016/j.actbio.2017.03.018
49. Shi MQ, Wen S, Zhang BX, et al. Micro/nano topography with altered nanotube diameter differentially trigger endoplasmic reticulum stress to mediate bone mesenchymal stem cell osteogenic differentiation. *Biomed Mater*. 2021;16(1):015024. doi:10.1088/1748-605X/abbfee